Sputter deposited nanocrystalline Ni and Ni-W films as catalysts for hydrogen evolution

M. Metikoš-Huković [a,*], Z. Grubač [b], N. Radić [c], A. Tonejc [d]

[a] Department of Electrochemistry, Faculty of Chemical Engineering and Technology, University of Zagreb, 10000 Zagreb, P.O. Box 177, Croatia
[b] Department of General and Inorganic Chemistry, Faculty of Chemical Technology, University of Split, N. Tesle 10, 21000 Split, Croatia
[c] Rudjer Boskovic Institute, Department of Materials Physics, 10002 Zagreb, P.O. Box 180, Croatia
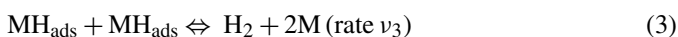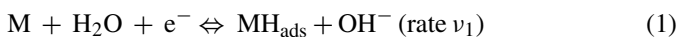[d] Faculty of Science, Department of Physics, 10002 Zagreb, Croatia

Abstract

Nanocrystalline nickel (nc-Ni) and Ni–W alloy coatings prepared by dc magnetron sputtering deposition method are very interesting materials due to their enhanced mechanical, catalytic and corrosion properties. The XRD analysis revealed that the grain-size of the as prepared Ni-films is about 10 nm. The Ni–W films exhibited microcrystalline structure in the examined composition range $Ni_{95}W_5$–$Ni_{75}W_{25}$. Their catalytic properties for the hydrogen evolution reaction (HER) were investigated in an alkaline electrolyte solution and comparative measurements were conducted on the electrodeposited Ni-electrode. The kinetic parameters deduced from linear polarization and electrochemical impedance spectroscopy (EIS) measurements indicated outstandingly high electrocatalytic activity of Ni–W and nc-Ni films. The best performance toward the HER demonstrates the $Ni_{90}W_{10}$ alloy in accordance with the prediction based on the electronic structure calculations and the enhanced density of states at the Fermi level of the 3d Ni band. Improved catalytic activity for the HER of nc-Ni in comparison with polycrystalline Ni was in accordance with 28% increase in the intercrystalline volume fraction at the very small grain size of sputter deposited Ni.
© 2006 Elsevier B.V. All rights reserved.

Keywords: Hydrogen evolution; Nanocrystalline Ni catalyst; Ni-W catalysts; Sputter deposition; Electrocatalysis

1. Introduction

Hydrogen evolution is one of the most investigated electrochemical reactions for which a modern theory of electrocatalysis has been developed. The reason is that the reaction proceeds through a limited number of steps with the only one type of intermediate. The well-known reaction steps in alkaline solutions are:

$$M + H_2O + e^- \Leftrightarrow MH_{ads} + OH^- \text{ (rate } \nu_1) \qquad (1)$$

$$MH_{ads} + H_2O + e^- \Leftrightarrow M + H_2 + OH^- \text{ (rate } \nu_2) \qquad (2)$$

$$MH_{ads} + MH_{ads} \Leftrightarrow H_2 + 2M \text{ (rate } \nu_3) \qquad (3)$$

HER starts with the proton discharge (Volmer reaction, Eq. (1)), and follows either the electrodesorption step (Heyrovsky reaction, Eq. (2)), or the H recombination step (Tafel reaction, Eq.

(3)). The distinction between steps (1), (2) and (3) as the rate-controlling is usually accomplished in terms of Tafel slopes or by calculating the rate constants of the forward and backward reactions through simultaneous fitting of polarization and impedance data. According to the general model for the HER mechanism, if the Volmer reaction (Eq. (1)) is the rate determining step (rds), the resulting Tafel curve should yield a slope of 118 mV dec^{-1} at 20 °C. If the Heyrovsky step is rate determining (Eq. (2)), the measured Tafel slope would yield a value of about 40 mV dec^{-1}, or 30 mV dec^{-1} for the Tafel desorption step (Eq. (3)).

Many papers have dealt with ways of increasing effectiveness of cathodes for the HER in alkaline solutions. Research has been mainly focused on several areas of interest: (i) intrinsic nature of the reaction, (ii) electrode composition, (iii) surface morphology, (iv) structural, chemical and electronic properties and (v) physical, chemical and electrochemical activation treatments.

The kinetics of H_2 evolution from alkaline solutions has been widely investigated on Ni, owing to its relatively good catalytic activity and high corrosion stability. There are two possibilities to enhance the activity of bare Ni: to increase the surface area by

* Corresponding author. Tel.: +385 1 4597 140; fax: +385 1 4597 139.
E-mail address: mmetik@marie.fkit.hr (M. Metikoš-Huković).

Nomenclature

A	area (cm^2)
a	Tafel intercept, related to the exchange current density, j_0
b_c	cathodic Tafel slope (mV dec^{-1})
C_{dl}	double layer capacitance (μF cm^{-2})
C_p	pseudo-capacitance (μF cm^{-2})
CPE	constant phase element (Ω^{-1} cm^2 s^n)
c	concentration (mol cm^{-3})
d	grain size (cm)
E	potential (V)
E_{OCP}	open circuit potential (V)
F	Faraday constant 96485 (C mol^{-1})
f	frequency (Hz)
j	current density (A cm^{-2})
j_0	exchange current density (A cm^{-2})
Q_p	parameter of CPE independent of frequency (F cm^{-2} s^{n-1})
R	gas constant, 8.314 (J K^{-1} mol^{-1})
R_{ct}	charge transfer resistance (Ω cm^2)
R_{el}	electrolyte resistance (Ω cm^2)
T	temperature (K)
Z	impedance Ω cm^2
z	number of electrons exchanged

Greek letters

α	symmetry factor
Δ	grain boundary thickness (cm)
η	overpotential (V)
ν	scan rate (mV s^{-1})
ω	angular frequency (rad s^{-1})

various methods or to alloy Ni with other metals to obtain alloys with optimal adsorption characteristics [1]. In recent years, there has been a substantial effort to investigate the structural, electronic and chemical properties of bimetallic systems. Bimetallic surfaces are extensively used in many industrial processes in the areas of catalisis, electrochemistry and microelectronics fabrication. Alloys are superior over single metal counterparts in terms of catalytic activity and/or selectivity.

The hydrogen evolution reaction is one of the most important electrochemical reactions, whereby proton from solution combine with electron at an electrode first to form hydrogen atoms chemisorbed at the electrode surface and then H$_2$ gas. The ability of a given metal to catalyze the HER is usually measured by the exchange current density, which is the rate of hydrogen evolution per surface area at the equilibrium electrode potential. Different metals have different exchange current densities. The hydrogen chemisorption energies have been used to understand the trends in the exchange current for HER. Volcano curves were obtained when measured exchange currents are plotted as a function of the calculated hydrogen adsorption energies [2–4].

The present work aims to investigate the electrocatalytic activity of sputter-deposited nanocrystaline Ni and binary Ni–W alloy coatings as catalyst for the HER in a 1 M NaOH at 30 °C by using the polarization and electrochemical impedance spectroscopy measurements. Particular attention was paid to the electrocatalytic behavior of investigated catalysts in dependence of the surface area and intrinsic properties of investigated catalysts in relation to a chemical disorder introduced by alloying Ni with W or a structural disorder introduced by grain boundaries in the nanostructured catalyst.

2. Experimental

Nc-nickel thin films were deposited by a dc magnetron sputtering onto alumina ceramic substrates at room/ambient temperature. The substrates rotated during deposition in order to avoid formation of a preferential stress axis. Base pressure in the process chamber was 10^{-6} to 10^{-5} Pa, and the working gas was argon at 10 mTorr in a continuous flow (30 sccm). Deposition rate was about 7–8 nm/min, and the film thickness was about 400 nm. The XRD analysis revealed that the grain-size of the as-prepared Ni-films is about 10 nm.

Binary Ni–W (5–25 at.% W) alloy films have been prepared by codeposition of pure nickel (99.99%) and pure tungsten (99.95%) in a multisource sputtering system CMS-18 supplied by Kurt J. Lesker Co. The base pressure in the process chamber was about 10^{-6} Pa, which increased a few times with cryopump throttled. High purity argon at 5 mTorr in a continuous flow mode was used as a working gas. Nickel target was mounted onto a magnetron source designed for sputtering of magnetic materials. Cathode power for nickel was kept the same (300 W) for all alloy compositions, while for tungsten cathode it was varied in the range of 17–102 W in order to cover the examined composition range. Deposition rate was about 15–20 nm/min and the final film thickness was in the 250–310 nm range. Circular (1 cm diameter) alumina ceramic substrates (and substrates made of other materials) were used. In order to obtain lateral compositional homogeneity of the alloys, the substrate holder rotated (10 rpm) during deposition. Substrates were not cooled, and probably attained somewhat higher temperature than the room temperature.

Electrodeposited nickel (ed-Ni) has been deposited on the carbon fibre microelectrode (CFM). The carbon microdiscs surface (0.014 cm^2) exposed to the electrolyte was thoroughly prepared by mechanical abrasion and subsequent polishing with alumina powder. The final cleaning was done by ultrasonication in redistilled water to remove polishing residues. In order to achieve a reproducible and active electrode surface, the electrode was anodically polarized in 0.5 M H$_2$SO$_4$ at 3.2 V against SCE for 25 s [5]. Nickel was deposited from 0.14 M solution of NiCl$_2$ at 55 °C by potentiostatic pulse technique. The potential of deposition was -1.170 V versus Ag/AgCl/3 M KCl electrode.

The electrocatalytic activity of as-prepared nanocrystaline Ni and Ni–W specimens for the HER was studied by using quasi-potentiostatic polarization and electrochemical impedance spectroscopy (EIS) techniques. Prior to each measurement, the surface of the working electrode ($A = 0.283$ cm^2) exposed to the electrolyte was degreased with ethyl alcohol and rinsed with redistilled water several times. A standard three-electrode cell

was utilized. The cell was a water-jacket version connected to a constant-temperature circulator. The counter electrode used in all measurements was a platinum sheet and the reference electrode to which all potentials in this paper were referred was Ag/AgCl; 3 M KCl electrode ($E_{Ag/AgCl} = 0.203$ V versus SHE at 30 °C). The measurements were carried out at 30 °C in a 1 M NaOH solution, deoxygenated by bubbling for 30 min with N_2 and then N_2 was passed over the solution. The experimental setup consisted of an EG&G PAR model 273A potentiostat/galvanostat and an EG&G PAR lock in amplifier, Model 5315. Quasi-potentiostatic polarization curves were recorded by sweeping the electrode potential from the reversible H^+/H_2 potential ($E_{rev}(H^+/H_2) = -1.01$ V versus Ag/AgCl electrode) in the cathodic direction at the scan rate of 1 mV s^{-1}. The solution resistance between the tested electrode and the reference electrode was determined by ac impedance measurement. Ohmic drop corrections, based on this resistance, were applied in all polarization measurements. The impedance spectra were recorded in a frequency region from 100 kHz to 50 mHz using 5 mV peak to peak amplitude. The applied dc potentials were located mainly in the linear portion of Tafel plots.

3. Results and discussion

3.1. Composition and structural characterization

Nanocrystalline Ni-film thickness was about 400 nm. The XRD analysis showed that the grain-size of the as-prepared Ni-films is about 10 nm. Chemical composition of the prepared Ni–W alloys is given as a nominal atomic fraction throughout the paper. It was estimated from the ratio of the deposition rates of pure nickel and pure tungsten, respectively, assuming bulk values for the density of deposited pure metals. It is well known that the deposition rate in a magnetron sputtering deposition is almost linear with the discharge power. However, it might slightly vary in (a prolonged) time due to the development of erosion tracks at the surface of the cathode.

The structure of the prepared films was examined by the XRD method, using Philips PW 1820 vertical goniometer with monochromatized Cu K_α-radiation. However, in order to avoid the interference with the diffraction pattern of the alumina substrate, the Ni–W films deposited simultaneously onto monocrystalline silicon were used to investigate the film structure. The same samples on Si-substrates were used in the Rutherford backscattering nuclear analysis of chemical composition of the as-prepared Ni–W alloys. Ni–W alloys are composed of solid solution of tungsten in the fcc-nickel and a small admixture of fine-grain phase of unresolved composition. The Ni(W) solid solution crystallites are preferentially (1 1 1) oriented in a direction perpendicular to the film plane. At the actual working gas pressure (5 mTorr), the prepared films are compressively stressed in a direction parallel to the film surface. Increased incorporation of somewhat greater tungsten atoms into the fcc-Ni grains and at the crystallites boundaries adds to the compressive stress, which is partially released through the expansion of the (1 1 1) interplanar spacing shown in Fig. 1.
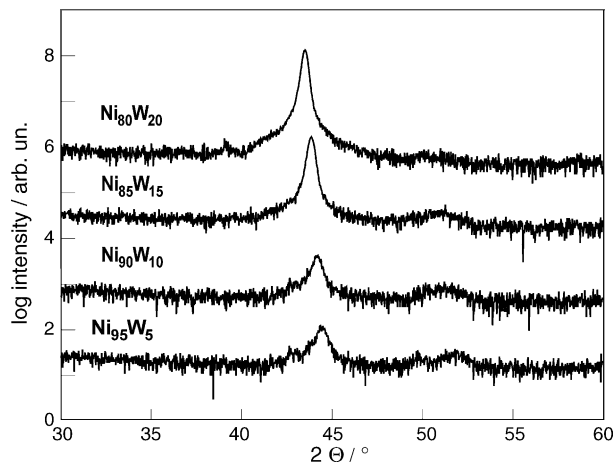

Fig. 1. The XRD patterns of Ni–W films deposited onto monocrystalline silicon.

3.2. Polarization measurements

Nickel and Ni-alloys are well known as good electrocatalysts to the HER and play an important role in various electrochemical processes [6–11]. The electrocatalytic performance of nc-Ni and Ni–W (5–25 at.% W) electrodes as a cathode material of long life stability in terms of hydrogen evolution in an alkaline solution was investigated using linear voltammetry and EIS techniques in an oxygen-free 1 M NaOH solution at 303 K. Comparative investigation has been performed on ed-Ni electrodes under the same experimental conditions. Quasi-potentiostatic polarization curves were recorded in the HER overpotential range between 0.0 and −0.4 V at the scan rate of 1 mV s^{-1}. Figs. 2 and 3 show typical results presented in log j against η coordinates which are suitable for the Tafel analysis based on the validity of the Butler-Volmer equation [12]:

$$j = j_0 \exp \frac{\alpha \eta F}{RT} = j_0 \exp \frac{\eta}{b_c} \tag{4}$$

where j is the current density, j_0 the exchange current density, α the charge transfer coefficient (used value was 0.5), η the overpotential, $\eta = E_j - E_r$, F the Faraday constant, R the gas
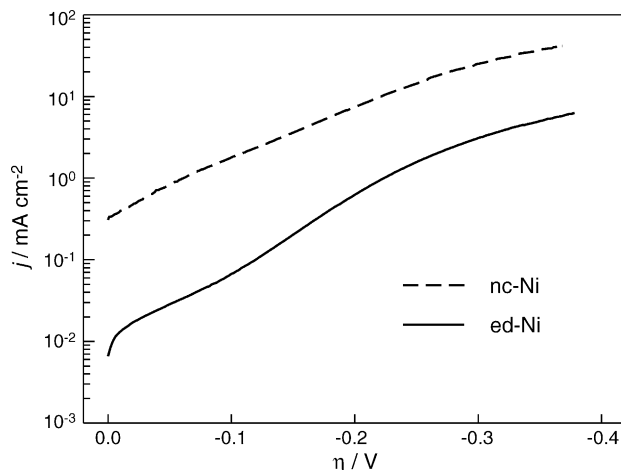

Fig. 2. Tafel polarization curves recorded on Ni coatings in 1.0 M NaOH solution at 30 °C. The scan rate was 1 mV s^{-1}.
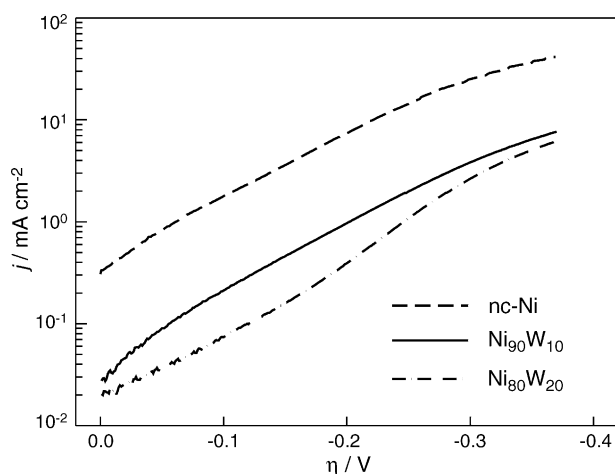
Fig. 3. Tafel polarization curves recorded on binary Ni–W alloy coatings in 1.0 M NaOH solution at 30 °C. The scan rate was 1 mV s^{-1}.

constant, T the absolute temperature, and b the Tafel slope [12]. The open circuit potential (E_{OCP}) of nc-Ni and ed-Ni is about -0.9 V, while for all investigated Ni–W alloys is about -0.5 V. Accordingly, E_{OCP} of the Ni–W system is more positive than the reversible potential of the HER, and also than that of corresponding thermodynamic potentials related to the oxidation of Ni and W: $E_{rev}(NiO/Ni) = -1.16$ V and $E_{rev}(WO_2/W) = -1.17$ V [13]. This point to the fact that at the E_{OCP} each of Ni–W electrodes is covered by a thin spontaneously formed oxide film [13], so called "natural" oxide which protect metal (alloy) against further dissolution (corrosion). During the cathodic polarization some of the "natural" oxide films formed on the surface of transition metals can be completely reduced [14,15], but the present results do not give sufficient information about that.

According to the general model for the HER mechanism, if the Volmer reaction step, Eq. (1), is rate determining, the resulting Tafel curve should yield a slope of 118 mV dec^{-1} at 20 °C. For nc-Ni and all investigated Ni–W alloy coatings the relatively high Tafel slopes (145–160 mV dec^{-1}) were obtained (see Table 1). The Tafel slope greater than $2.3 \times 2RT/F = 118$ mV is frequently observed for the HER proceeding on "natural" oxide-covered valve metals such as Al [16] or other valve metals (Ta, Nb, Ti, W, Zr, ...) [17]. Similar observation has been reported on Ni-based catalysts [6,18,19]. Thus,

$$\frac{\partial \eta}{\partial \log j} = \frac{2.3RT}{\alpha z F (1 - \partial \eta_f / \partial \eta)} \equiv \text{Tafel slope} \qquad (5)$$

where η_f is the fraction of the total overpotential, η which operates across the electronically conducting oxide film. The Tafel slope of 160 mV dec^{-1} yields $\eta_f = 0.26\eta$ for $\alpha = 0.5$ and $z = 1$. This is, in turn, related to the symmetry factor, α, the value of which then decreases, assuming that the reaction mechanism does not change. Note that for the Volmer step as the RDS, the symmetry factor, α, is equal to the transfer coefficient, α_a. For the ed-Ni electrode, the "intrinsic" Tafel slope of about 105 mV dec^{-1} slightly deviates from the theoretical value. The corresponding $\alpha_a = 0.58$ suggests an improvement of charge transfer kinetics of the HER at overpotentials ranging from 0 up to 0.20 V on the freshly prepared Ni-electrodeposit

Table 1
Kinetic parameters for the HER on nc-Ni and ed-Ni electrodes in 1.0 M NaOH solution at 30 °C deduced from (A) polarization curves and (B) electrochemical impedance spectroscopy measurements

	A		B	
	$-b_c$ (mV)	j_0 (μA cm^{-2})	$-b_c$ (mV)	j_0 (μA cm^{-2})
Nc-Ni	160	307	157	57
Ed-Ni	105	11	105	11

Table 1(A) and 2(A) summarize the kinetic parameters, the Tafel slope, b_c, and the exchange current density, j_0, obtained from polarization measurements. Current densities which characterize the rate of the HER on nc-Ni, ed-Ni and Ni–W films, have been calculated using the geometric area of the each investigated electrode. The highest exchange current densities (j_0) presented in Tables 1 and 2, determined on the nc-Ni electrode and on the Ni$_{90}$W$_{10}$ alloy, point that these catalysts are the most active for the HER among the catalysts investigated. Compared to ed-Ni electrode as well as to pure polycrystalline Ni [6,20] all investigated Ni–W alloys yielded better catalytic performance towards H$_2$ evolution.

3.3. Impedance spectroscopy measurements

The impedance data were collected at selected potentials located mainly in the linear portion of the Tafel plots, at overpotentials ranging from -0.05 to -0.20 V.

Fig. 4 shows impedance spectra recorded on the nc-Ni electrode and Fig. 5 impedance spectra recorded on the Ni$_{90}$W$_{10}$ electrode, presented in the form of Nyquist and Bode plots (the logarithm of overall impedance modulus, log $|Z|$ and the phase angle, Θ against the logarithm of frequency, log f). In Bode plots, at intermediate frequencies a linear dependence of log $|Z|$ against log f and the well-defined maximum observed in the phase angle, Θ against log f plots, indicate a capacitive behavior of the electrode. The Faradaic resistance R_F dominates at lowest frequencies and can be determined from the low frequency impedance plateau ($R_{el} + R_F$) where R_{el} is the electrolyte resistance (cca 1 Ω cm^{-2}). It should be noted that the Faradaic resistance continuously decreases with increasing overpotential, as follows from Figs. 4 and 5 and Tables 3 and 4.

Table 2
Kinetic parameters for the HER on Ni–W alloys in 1.0 M NaOH solution at 30 °C deduced from (A) polarization curves and (B) electrochemical impedance spectroscopy measurements

W (at.%)	A		B	
	$-b_c$ (mV)	j_0 (μA cm^{-2})	$-b_c$ (mV)	j_0 (μA cm^{-2})
5	162	25	175	29
7.5	161	43	175	45
10	154	50	172	56
12.5	146	26	172	32
15	163	25	177	31
20	155	17	156	22
25	158	30	179	16

Table 3
Impedance parameters for the HER in a 1 M NaOH solution

η (mV)	$10^6 \times C_{dl}$ (F cm^{-2})	$10^6 \times Q_p$ (Ω^{-1} cm^2 s^n)	n_p	$R_{ct} + R_p$ (Ω cm^2)
Nc-Ni				
−50	1950	1210	0.827	96
−100	1360	871	0.860	64
−150	1070	1080	0.905	29
−200	920	3060	1.000	11
Ed-Ni				
−50	3.00	168	0.694	493
−100	2.90	145	0.704	153
−150	2.50	129	0.705	61
−200	2.00	105	0.723	30

$R_{el} = 2\ \Omega\ \text{cm}^2$.

Table 4
Impedance parameters for the HER on nc-Ni and Ni–W electrodes in a 1 M NaOH solution

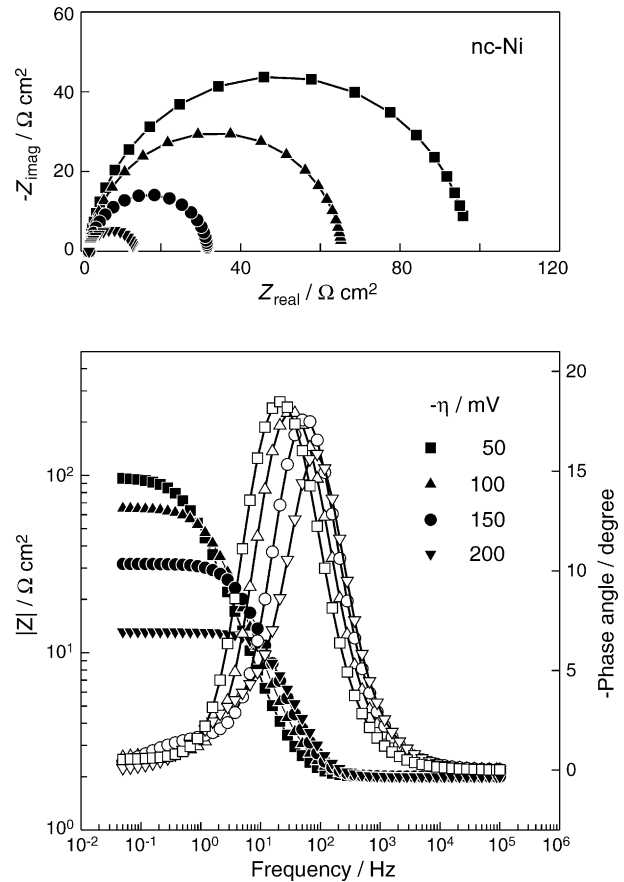| η (mV)	$10^6 \times C_{dl}$ (F cm^{-2})	$10^6 \times Q_p$ (Ω^{-1} cm^2 s^n)	n_p	$R_{ct} + R_p$ (Ω cm^2)
Ni$_{95}$W$_5$				
−50	0.91	2610	0.948	225
−100	0.94	1790	0.961	148
−150	0.90	1330	0.959	81
−200	0.98	1190	0.950	36
Ni$_{92.5}$W$_{7.5}$				
−50	0.49	3510	0.940	156
−100	0.50	2450	0.942	85
−150	1.70	1790	0.943	46
−200	0.84	1580	0.941	25
Ni$_{90}$W$_{10}$				
−50	1.07	3690	0.927	119
−100	0.52	2960	0.929	64
−150	1.19	2460	0.925	33
−200	1.79	2260	0.921	17
Ni$_{87.5}$W$_{12.5}$				
−50	1.47	2140	0.937	197
−100	1.71	1560	0.947	117
−150	1.70	1230	0.946	64
−200	1.89	1140	0.937	29
Ni$_{85}$W$_{15}$				
−50	2.29	2370	0.941	207
−100	1.48	1710	0.944	128
−150	1.77	1280	0.944	71
−200	1.77	1180	0.936	32
Ni$_{80}$W$_{20}$				
−50	2.21	1530	0.926	264
−100	1.97	1210	0.932	136
−150	1.39	1050	0.922	66
−200	2.29	940	0.921	28
Ni$_{75}$W$_{25}$				
−50	1.09	259	0.793	362
−100	1.21	239	0.842	246
−150	1.11	254	0.861	136
−200	1.33	298	0.883	52

$R_{el} = 2\ \Omega\ \text{cm}^2$.

Fig. 4. Impedance spectra (Bode plots) of the nc-Ni electrode for the HER in 1.0 M NaOH solution at various overpotentials.

Experimental data were modeled by the electrical equivalent circuit (EEC) $R_{el}(C_{dl}(R_{ct}(C_pR_p)))$ proposed by Armstrong and Henderson [21], where R_{ct} is the charge transfer resistance, C_{dl} is the double layer capacitance, R_p is the resistance related to the hydrogen adsorption, usually called the pseudo-resistance, and C_p is the pseudo-capacitance. The Faradaic impedance Z_f is defined as:

$$Z_f = R_{ct} + \frac{R_p}{1 + j\omega\tau_p} \qquad (6)$$

where ω is the frequency and $\tau_p = R_pC_p$ is the time constant related to the relaxation process when the overpotential is changed [22].

In order to obtain better fitting, a parameter Q_p of the constant phase element, CPE was used instead of C_p. The data were fitted using the complex non-linear least squares (CNLS) fit analysis software written by Boukamp [23]. Table 3 contains the values of impedance parameters for all investigated electrodes. A standard deviation χ-quadrate was in the order of 10^{-5}, and the relative error of each element was less then 5% suggesting a very good agreement between experimental and theoretical data.

At all selected potentials the sum of $R_{ct} + R_p$ represents the total Faradaic resistance of the working electrode, R_F, and its reciprocal is directly related to the HER current density at the corresponding potential. For all investigated catalysts a linear relationship E versus $\log(R_{ct} + R_p)^{-1}$ is observed (see
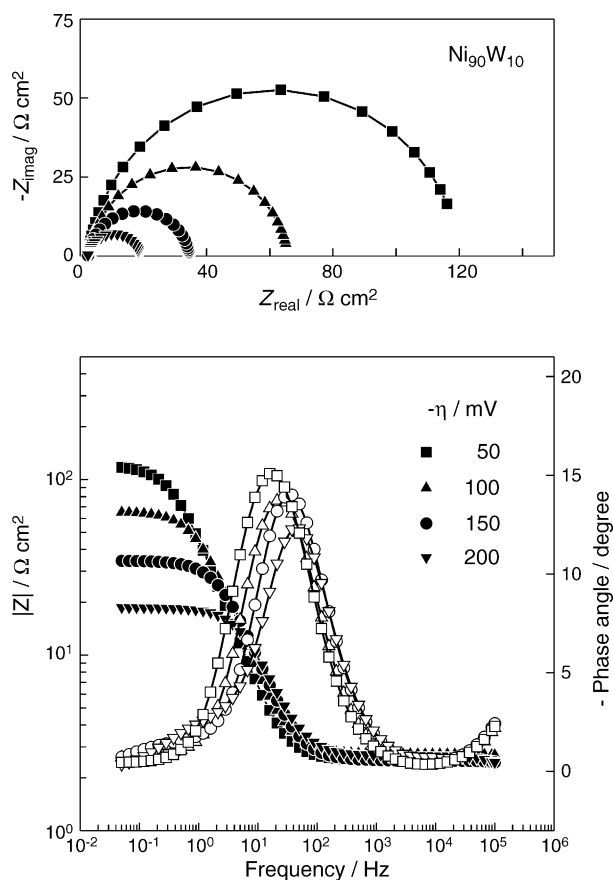
Fig. 5. Impedance spectra (Bode plots) of the $Ni_{90}W_{10}$ electrode for the HER in 1.0 M NaOH solution at various overpotentials.

Figs. 6 and 7). The intercepts of these lines at the 0 overpotential yield the exchange current densities, j_0 tabulated in Tables 1(B) and 2(B), together with the Tafel slopes, b_{EIS}. Tafel slopes for Ni–W alloys (Table 2(B)) are slightly higher than those obtained from the quasi-potentiostatic dc measurements (Table 2(A)). This difference could be influenced by experimental conditions. Namely, during potentiostatic EIS measurements the electrode is kept ca. 15 min at a selected potential due to
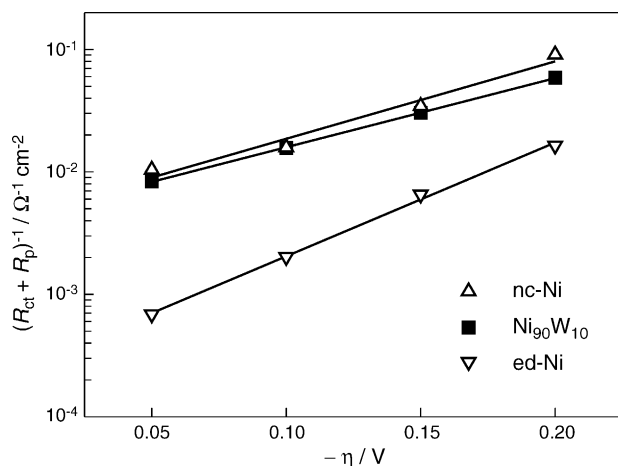

Fig. 6. $(R_{ct} + R_p)^{-1}$ against η relationships for the HER on nc-Ni, ed-Ni and $Ni_{90}W_{10}$ alloy in 1.0 M NaOH solution at 30 °C, obtained from data in Table 3.

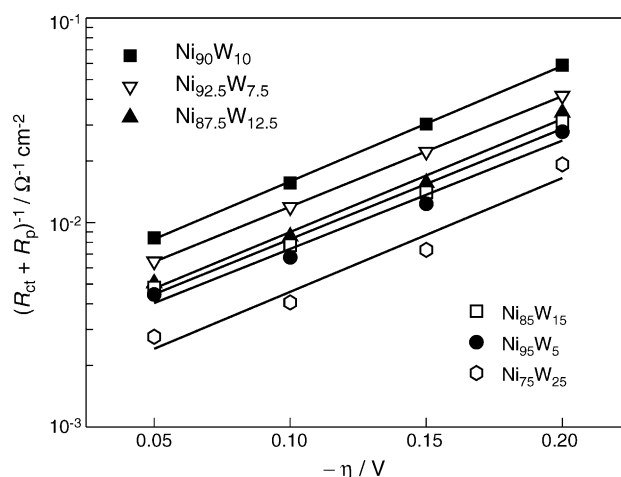Fig. 7. $(R_{ct} + R_p)^{-1}$ against η relationships for the HER on Ni–W alloys in 1.0 M NaOH solution at 30 °C, obtained from data in Table 3.

the data collection in the wide range of frequencies and during this period the hydration of electrodes takes place. The "natural" oxide partially transforms to a hydride which further suppresses H adsorption. In terms of the exchange current density, j_0, determined from dc and ac measurements (Table 1) it is clear that the $Ni_{90}W_{10}$ alloy and nc-Ni yield the highest intrinsic electrocatalytic properties for the HER. All investigated Ni–W alloys are also very active catalysts, showing a superior catalytic activity for the HER when compared to pure polycrystalline Ni [6] or electrodeposited Ni [20]. A general explanation of catalytic activity of transition metal-based alloys for H_2 evolution is related to the electronic structure of both the host metal and alloying component. The most active alloy coating is exactly the one that gives the highest electron density for the HER. The d-band has been claimed as crucial in electrocatalysis of the HER (it represents both bonding and adsorptive band), while the overall kinetics of the HER has been, on the other hand, influenced by the electronic density of states at the Fermi level.

3.4. The effect of alloying

The mechanism for electrolytic evolution of hydrogen is usually discussed in terms of various physical and/or electronic parameters.

The theoretical approach to explain the HER catalytic activity of alloys is complex, and several theories have been proposed. The theory of alloying effect of transition metal-based alloys has been discussed by Jakšić [24,25] on the basis of the Engel–Brewer valence-bond theory, as a generalized Lewis acid–base reaction model that is frequently cited in literature [26]. It has been postulated that the intermetallic combination of transition elements, having partially or half-filled d-orbital (e.g. Mo, W, V, etc.), with transition metals, having internally paired d-electrons (e.g. Ni, Pd, Pt, Co, etc.), results in a significant change in their bonding strength, and, consequently, increased intermetallic stability, whose maximum usually coincides with optimal d^8-electrons for the synergism and maximal activity for the HER. The theory (concept) proposed by Jakšić has been sup-

ported by a number of experimental studies related to the HER electrocatalysis [1,25,27]. Another theory (concept) related to the synergism of the HER on bimetallic catalysts has been postulated by Ezaki et al. [28–30]. Ezaki's concept was based on experiments on the hydrogen overpotential and its interpretation using the electronic structure calculated by the DV–Xα cluster method [31].

The main difference between these two concepts is in the direction of electron transfer between a base metal and an alloying element. Namely, if the alloying element is less electronegative (for example Mo, W) than the host metal (for example Co, Ni), the charge transfer occurs from the alloying element to the host metal. In this case, excess of electrons is located near the host metal atoms creating electronic configuration suitable for electron adherence and transference during the HER. The hydrogen overpotential of the alloy is close to that of the host metal. Accordingly, Ni–Mo, Ni–W, Ni–Ti alloys would, in principle, offer the best catalytic properties toward hydrogen evaluation.

In order to gain a decisive insight into the mechanism of the HER and the ways how it may be facilitated, the electronic structure of metal and its change due to various alloying constituents are of interest. Some of the most revealing theoretical and experimental data, concerning the electronic structure of metals and alloys result from the density functional theory calculations [32,33] and the magnetization measurements [34–38]. A somewhat different view from above discussed concepts is offered by the theoretical results calculated by the tight-binding linear muffin-tin-orbital (TM-LMTO), atomic sphere approximation (ASA) method [39] that has been successfully applied to rare earth and transition metals and, in particular, to some alloys of special interest for the HER. To our knowledge, this method has not been applied to the Ni–W system, but some parallels may be drawn with the Co–W system as its functional analog. Szapunar et al. [32] provided the results of calculations for the Co–W and Ni–P systems in the form of: the spin polarized and localized density of states at and around the Fermi level, saturation magnetization and magnetization contributions of the local moments of all s, p and d electrons. Correlation of calculated results with the magnetization experimental data is well documented, but contrary to rigid band theory, the negligible charge transfer has been calculated, e.g. of 0.03 and 0.06 electrons for 10 wt.% and 20 wt.% W, respectively. Hence, detailed calculations reveal a more complex mechanism than the Brewer–Engel theory would predict indicating that the increase in the electrochemical activity should be ascribed to the overall modification of the density of states of the host metal rather than to the electron transfer.

The saturation magnetization measurements and electronic structure calculation demonstrated that d-band vacancy of Ni in Ni–Mo and Ni–W alloys decreases with addition of Mo or W and becomes nearly 0 at about 11 at.% Mo and 8 at.% W. This was in good agreement with the fact that the optimum surface composition of both sputter deposited alloys for the HER activity in 1 M NaOH was that of about 10 at.% Mo or W [40]. Ezaki et al. [41] have demonstrated a continuous rise of HER activity with increasing Mo content from 0 to 10 at.% in Ni–Mo UFP electrodes. According to Kawashima [40], in order

to obtain more active electrodeposited Ni-alloy catalyst for the HER, the threshold concentration of Mo should be 15 at.% and for W 19 at.%. It is noteworthy that the "threshold" values can be influenced by the inherent limitations of the electrodeposition process and pH value. The influence of alloying Ni with left-hand side transition metals (Fe, Mo, W) on the electrocatalytic activity for the HER was investigated in an acid environment [20]. Ni–Mo (12 at.% Mo) and Ni–W (20 at.%) W) electrodeposits were found to yield the highest intrinsic electrocatalytic activity, which was explained with modification of electron density of d orbitals by alloying Ni with Mo and W.

The results presented in Fig. 8 show how the electrocatalytic activity of investigated Ni–W alloys for the HER depends on the W content in the Ni–W alloy. The exchange current density, j_0 rises with increasing W content in the alloy and becomes maximal at $c(W) = 10$ at.%. A comparison of this trend with the calculated and experimental saturation magnetization values in Co–W alloys, as a function of W content, has shown that the theory adequately describes the effect of chemical disorder (introduced by alloying) on the catalytic activity of Ni–W alloys. It should be stressed that the main contribution to the density of states and magnetic moments comes from d-electrons. According to the results of the TB-LMTO, ASA method used to calculate the electronic structure of the transition metal alloys, based on the local density-functional theory, the highest activity for the HER can be expected at the alloy composition of about 10 at.% W. The optimal catalytic activity for the HER on the Ni–W alloy containing 10 at.% W coincides with an increase in the density of states at Fermi level $D(E_F)$ of the 3d Ni band. The increased electron density around Ni-sites influences proton discharge at the Ni–W surface according to the Eq. (1) and Ni-sites can serve as a hydrogen source for the neighboring W sites. Tungsten sites in Ni–W alloys act as the "traps" for hydrogen where the ion/atom recombination and molecular hydrogen desorption, Eq. (2), is promoted more efficiently. The H-trapping function of W also protects the alloy from deactivation [18].

Here a brief comment on surface composition of the examined alloys is due. It seems that the forces governing the surface
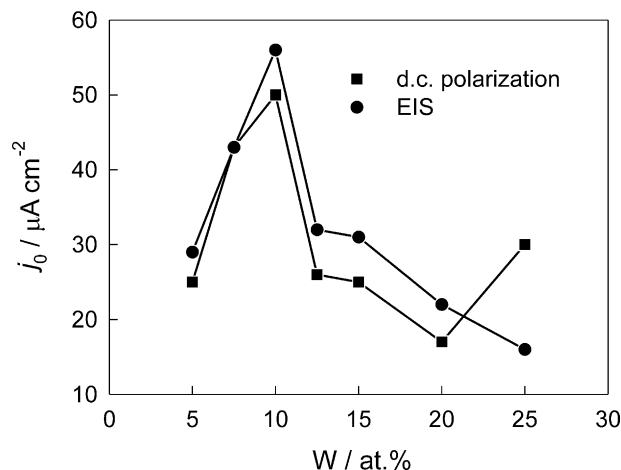

Fig. 8. The dependence of the exchange current density, j_0 obtained from EIS (●) and polarization (■) measurements on the content of W in the coating.

segregation in the solid solutions of tungsten in nickel are delicately balanced (ref. [42]). Thus, a very few available experimental results (by the XPS method) are inconclusive: the results presented in (ref. [40]) indicate depletion of tungsten in the surface layer of Ni-(19–60)at.%W alloys prepared by cosputtering, while investigation of the Ni-7%W solid solution under a well-controlled conditions (ref. [42]) has shown an intrinsic tendency (enhanced by oxygen adsorption) of tungsten to segregate to the free surface. The surface composition of the actual Ni(5–25 at.%W) sputter-deposited solid solutions has not been examined separately. However, assuming that the most active Ni–W alloy is exactly the one that gives the highest electron density (at the Fermi level) for the HER, a simple comparison between the calculated (ref. [43]) total electron density at E_F, and bulk Ni–W alloy composition at which the highest HER activity was observed, might suggest/indicate a tungsten segregation at the surface of the Ni-10 at.%W bulk alloy.

3.5. Nanocrystalline nickel (nc-Ni)

Nanocrystalline nickel electrode demonstrates better electrocatalytic performance toward the HER than the bulk [6] or electrodeposited Ni electrode (see j_0 values in Table 1), and comparable catalytic properties to that of the $Ni_{90}W_{10}$ alloy (see j_0 values in Table 2). Explanation lies in the difference between microstructure of nanocrystalline materials and their conventional polycrystalline and amorphous counterparts. This is mainly due to the increase in the intercrystalline volume fraction, especially at the very small grain sizes [44–46]. The intercrystalline volume (the product of the total grain boundary area and the grain boundary thickness) corresponds to the volume of the material that is affected by the structural disorder associated with grain boundaries. Assuming a regular 14 sides tetra decahedron as a grain shape, the intercrystalline volume fraction (fic) can be calculated from the following equation [44]:

$$fic = 1 - \left[\frac{(d - \Delta)}{d} \right]^3 \qquad (7)$$

where d is the grain size and Δ the grain boundary thickness.

It has been shown that the several physical properties of nanocrystalline materials exhibit significant difference [44,45] in comparison to their conventional counterparts.

Double layer capacitance, C_{dl} as well as pseudocapacitance, C_p (Q_p) for the nc-Ni electrode and the ed-Ni electrode, presented in Table 3, differ markedly. C_{dl} for the nc-Ni electrode is a three orders of magnitude higher than C_{dl} for the ed-Ni electrode (see Table 3, $\eta = -100$ mV). Drastic increase in the double layer capacitance and pseudocapacitance can be related to the 28%-ig increase of the intercrystalline volume fraction in the nanocrystalline Ni material having the grain size of 10 nm. In the ed-Ni material with grain size >100 μ the intercrystalline volume fraction equals 0%.

In the frame of above discussion concerning drastic change of magnetization of transient metal alloys by a chemical disorder introduced by alloying Ni with Mo(W) it is noteworthy that a structural disorder introduced by grown boundaries in the nanostructured Ni-alloys has little effect on their saturation magnetization.

4. Conclusions

Binary Ni–W alloy (5–25 at.%) coatings (250–310 nm) on alumina ceramic have been prepared by dc magnetron sputtering codeposition. The composition of the prepared films is determined by the Rutherford Backscattering nuclear analysis. It was found that up to the 15 at.% tungsten content, the measured chemical composition of the film is within a fraction of the atomic percent of the nominal tungsten content. Only at higher tungsten concentrations a noticeably departure was found: nominal 20 at.% W corresponds to 21.2 at.% by the RBS, and nominal 25 at.% W corresponds to 27.5 at.% as determined by the RBS.

The XRD analysis revealed that prepared Ni–W films exhibit predominantly microcrystalline structure in the examined composition range. The XRD analysis revealed that the grain-size of the nc-Ni films is about 10 nm.

The kinetic parameters, indicative for the high HER activity, were determined using the linear polarization and the electrochemical impedance spectroscopy techniques. Presented results clearly demonstrate that alloying nickel with tungsten causes an increase in the electrocatalytic activity for the HER in comparison to pure polycrystalline bulk and electrodeposited nickel. The Ni 10 W alloy was found to yield the highest intrinsic electrocatalytic activity, which was explained by modifying the electron density of states at the Fermi level of Ni upon alloying it with tungsten. It was also pointed that the synergistic effect can contribute to an increased electrocatalytic activity. A simple cooperative functioning of the alloy components occurs via the spillover process.

Nanocrystalline Ni-electrode demonstrated almost the same catalytic performance toward the HER as the $Ni_{90}W_{10}$ alloy. Improved catalytic activity for the HER of nanocrystalline Ni in a comparison with polycrystalline Ni was explained with microstructural characteristics of nano-materials.

Acknowledgements

References

[1] J.M. Jakšić, M.V. Vojnović, N.V. Krstajić, Electrochim. Acta 45 (2000) 4151.
[2] S. Trasatti, J. Electroanal. Chem. 39 (1972) 163.
[3] J.O.'M. Bockris, A.K.N. Reddy, M. Gamboa-Aldeco, Modern Electrochemistry, second ed., Kluver Academic/Plenum Publishers, New York, 2000, p. 1285.
[4] J.K. Norskov, T. Bligaard, A. Logadottir, J.R. Kitchin, J.G. Chen, S. Padelov, U. Stimming, J. Electrochem. Soc. 152 (2005) 123.
[5] A. Dekanski, J. Stevanović, R. Stevanović, B.Ž. Nikolić, V.M. Jovanović, Carbon 39 (2001) 1195.
[6] M. Metikoš-Huković, A. Jukić, Electrochim. Acta 45 (2000) 4159.
[7] P. Los, A. Rami, A. Lasia, J. Appl. Electrochem. 23 (1993) 135.

[8] C. Hitz, A. Lasia, J. Electroanal. Chem. 500 (2001) 213.

[9] S.N. Tanaka Hirose, T. Tanaki, Int. J. Hydrogen Energy 25 (2000) 481.

[10] N.V. Krstajić, B.N. Grgur, N.S. Mladenović, M.V. Vojnović, M.M. Jakšić, Electrochim. Acta 42 (1997) 323.

[11] J. Panek, A. Serek, A. Budniok, E. Rowinski, E. Lagiewka, Int. J. Hydrogen Energy 28 (2003) 169.

[12] J.O.'M. Bockris, S.U.M. Khan, Surface Electrochemistry: A Molecular Level Approach, Plenum Press, New York, 1993, Chapter 3, p. 211.

[13] M. Pourbaix, Atlas of Electrochemical Equilibria in Aqueous Solutions, Pergamon Press, Oxford, 1966.

[14] A.K. Vijh, J. Electrochem. Soc. 116 (1969) 972.

[15] Z. Grubač, M. Metikoš-Huković, Electrochim. Acta 43 (1998) 3175.

[16] M. Metikoš-Huković, R. Babić, Z. Grubač, S. Brinić, J. Appl. Electrochem. 24 (1994) 772.

[17] J.W. Diggle, A.K. Vijh, Oxide and Oxide Films, 4, Marcel Dekker, New York, 1976.

[18] J.G. Highfield, E. Claude, K. Oguro, Electrochim. Acta 44 (1999) 2805.

[19] B. Losiewicz, A. Budniok, E. Rowinski, E. Lagiewka, A. Lasia, Int. J. Hydrogen Energy 29 (2004) 145.

[20] E. Navarro-Flores, Z. Chong, S. Omanović, J. Mol. Catal. A-Chem. 226 (2005) 179–197.

[21] R.D. Armstrong, M. Henderson, J. Electroanal. Chem. 39 (1972) 81.

[22] N. Krstajić, M. Popović, B. Grgur, M. Vojnović, D. Šepa, J. Electroanal. Chem. 512 (2001) 16.

[23] B.A. Boukamp, Equivalent circuit user's manual, report CT88/265/128, University of Twente, Department of Chemical Technology, Netherland, 1989.

[24] M.M. Jakšić, Int. J. Hydrogen Energy 26 (2001) 559.

[25] M.M. Jakšić, C.M. Lačnjevac, B.N. Grgur, N.V. Krstajić, J. New Mater. Electrochem. Syst. 3 (2000) 169.

[26] G. Lu, P. Evans, G. Zangari, J. Electrochem Soc. 150 (2003) 551.

[27] N.V. Krstajić, B.N. Grgur, N.S. Mladenović, M.V. Vojnović, M.M. Jakšić, Electrochim. Acta 42 (1997) 323.

[28] H. Ezaki, M. Morinaga, S. Watanabe, Electrochim. Acta 38 (1993) 557.

[29] H. Ezaki, M. Morinaga, S. Watanabe, J. Saito, Electrochim. Acta 39 (1994) 1769.

[30] H. Shibutani, T. Higashijima, H. Ezaki, M. Morinaga, K. Kikuchi, Electrochim. Acta 43 (1998) 3235.

[31] T. Nambu, H. Ezaki, M. Takagi, H. Yukawa, M. Morinaga, J. Alloys Comp. 330 (2002) 318.

[32] B. Szpunar, M. Aus, C. Cheung, U. Erb, G. Palumbo, J.A. Szpunar, J. Magn. Mater. 187 (1998) 325.

[33] M. Hanson, H.J. Bauer, J. Alloys Comp. 179 (1992) 339.

[34] F.A. Khan, M.A. Asgar, P. Nordblad, J. Magn. Mater. 174 (1997) 121.

[35] M.V. Ananth, N.V. Partasardhy, Mater. Sci. Eng. B 55 (1990) 451.

[36] A. Stephen, T. Nagarajan, M.v. Ananth, Mater. Sci. Eng. B55 (1998) 184.

[37] A. Burgstaller, W. Socher, J. Voitländer, I. Bakonyi, E. Tóth-Kádár, A. Lovas, H. Ebert, J. Magn. Mater. 109 (1992) 117.

[38] S.S.M. Tavares, S. Miraglia, A. Lafuente, D. Fruchart, J. Magn. Mater. 242–245 (2002) 898.

[39] O.K. Andersen, O. Jelsen, M. Sob, in: M. Yussouf (Ed.), Electronic Band Structure and its Application, Springer Verlag, Berlin, 1980, pp. 1–57.

[40] A. Kawashima, E. Akiyama, H. Habazaki, K. Hashimoto, Mater. Sci. Eng. A 226–228 (1997) 905.

[41] H. Ezaki, T. Nambu, M. Morinaga, M. Udaka, K. Kawasaki, Int. J. Hydrogen Energy 21 (1996) 877.

[42] A. Sagie, M. Polak, Surf. Sci. 459 (2000) 223–229.

[43] S.I. Simak, A.V. Ruban, Yu.H. Vekilov, Solid State Comm. 87 (1993) 393–396.

[44] H. Gleiter, Prog. Mater. Sci. 33 (1989) 223.

[45] U. Erb, Nanostruct. Mater. 6 (1995) 533.

[46] G. Palumbo, S.J. Thorpe, K.T. Aust, Scripta Metall. 24 (1990) 1347.